Acta Metall. Sin. (Engl. Lett.), 2018, **31**, 134–142
https://doi.org/10.1007/s40195-017-0626-z

Origin of Insignificant Strengthening Effect of CNTs in T6-Treated CNT/6061Al Composites

Ke Zhao[1,2] · Zhen-Yu Liu[1] · Bo-Lyu Xiao[1] · Ding-Rui Ni[1] · Zong-Yi Ma[1,3]

Received: 15 April 2017 / Revised: 21 June 2017 / Published online: 8 July 2017
© The Chinese Society for Metals and Springer-Verlag GmbH Germany 2017

Abstract Carbon nanotube (CNT)-reinforced 6061Al (CNT/6061Al) composites were fabricated via powder metallurgy combined with friction stir processing (FSP). CNTs were dispersed after FSP and accelerated the precipitation process of the CNT/6061Al composites. However, the strengthening effect of CNTs on the T6-treated materials was insignificant, while the composites under the FSP and solution treatment conditions exhibited increased strength compared to the matrix. Precipitate-free zones (PFZs) were detected around CNTs in the T6-treated CNT/6061Al composites, and a model was proposed to describe the effect of PFZs on strength. The calculations indicated that the strength of PFZs was similar to that of the T6-treated 6061Al. As a result, the strengthening effect of CNTs on the T6-treated CNT/6061Al composites was insignificant.

KEY WORDS: Metal matrix composites; Carbon nanotubes; Precipitate-free zones

1 Introduction

Carbon nanotube (CNT) has attracted growing attentions for its low density, superior mechanical and physical properties [1–4]. Due to these attractive properties, CNT is considered as a promising reinforcement for composites [5–7]. In the past decades, CNT/Al composites have received a lot of focus due to the significantly enhanced properties [5, 8].

The key issue to produce the CNT/Al composites with superior properties is achieving the homogenous dispersion of CNTs in the aluminum matrix [9–15]. To disperse the entangled CNTs, various methods have been exploited, such as ultrasonic [15], high-energy ball milling [16–18], flaky powder metallurgy [19, 20], molecular-level mixing [13, 21] and friction stir processing (FSP) [22–24].

FSP, a relatively new method of fabricating metal matrix composites, has been used to disperse CNTs into the aluminum matrix [22, 25–28]. Compared with other fabrication methods, FSP introduced little contamination during the fabrication process and induced limited damage to CNTs. Therefore, the CNT/Al composites with high tensile strength as well as good physical properties could be achieved by FSP combined with powder metallurgy (PM) route [8, 12]. In our previous studies [12, 27, 28], CNT/Al, CNT/6061Al and CNT/2009Al composites have been successfully fabricated in this route, and significant reinforcing effect of CNTs has been achieved.

Available online at http://link.springer.com/journal/40195

✉ Bo-Lyu Xiao
blxiao@imr.ac.cn

✉ Zong-Yi Ma
zyma@imr.ac.cn

[1] Shenyang National Laboratory for Materials Science, Institute of Metal Research, Chinese Academy of Sciences, Shenyang 110016, China

[2] University of Chinese Academy of Sciences, Beijing 100040, China

[3] Key Laboratory of New Processing Technology for Nonferrous Metal and Materials, Ministry of Education, Guilin University of Technology, Guilin 541004, China

However, in previous studies little attention has been focused on the heat treatment behavior of the CNT/Al composites [21, 29], though heat treatment is very important for some aluminum alloy matrix composites. Up to now, the effect of CNTs on the aging behavior of aluminum alloys matrix composites has only been reported in limited investigations [21, 29–32]. Nam et al. [21] fabricated CNT/Al–4Cu composites by molecular mixing combined with PM and investigated the aging behaviors of the composites. They found that CNTs had no effect on the distribution of alloy element, but CNTs accelerated the precipitation process. In another study [29], Mg depletion was detected around CNTs in CNT/6063Al composites and decreased the amount of precipitates in the matrix after aging, leading to no strengthening effect of the aged composites. However, in that study, CNTs were not homogenously distributed in the matrix. Furthermore, the precipitation acceleration effect of CNTs was not considered so that the T6-treated CNT/6063Al composites might not reach the aging peak.

Clearly, the knowledge of the effect of CNTs on the aging behavior and the mechanical properties of the aged CNT/Al composites is still lacking and further investigation is necessary. In this study, the CNT/6061Al composites were fabricated by FSP combined with the PM process. The microstructure and mechanical properties of the CNT/6061Al composites under different heat treatment conditions were investigated. The aim is to understand the effect of CNTs on aging response and to optimize the mechanical properties of the CNT/6061Al composites by heat treatment.

2 Experimental

2.1 Fabrication of the CNT/6061Al Composites

The as-received 6061Al (Al–1.1Mg–0.56Si–0.2Cu, wt%) powders having a spherical shape with an average diameter of about 10 μm were used as the matrix. The as-received CNTs having an entangled morphology with an outer diameter of 20–40 nm and a length of 2–5 μm were used as the reinforcement. The composites with CNT contents of 0, 1.5, and 3 vol% were fabricated by powder metallurgy technique.

CNTs were mixed with the 6061Al powders in a mechanical mixer at 50 r/min with a ball to powder ratio of 1:1 for 8 h. No pre-treatment was conducted on CNTs. The mixed composite powders were cold-compacted in a die, degassed and vacuum hot-pressed into cylindrical billets at 853 K. The billets were hot-forged into disk plates and then subjected to 4-pass in situ FSP at a tool rotation rate of 1200 rpm and a travel speed of 100 mm/min. The fabrication details could be found in our previous studies [8, 26, 27]. All specimens used in this study were machined from the FSP zones.

For obtaining the strength data for model calculation, 1.5 vol% CNT-reinforced pure Al (CNT/Al) composite and pure Al samples were also fabricated with the same process parameters.

2.2 Heat Treatments of the CNT/6061Al Composites

The CNT/6061Al composites and 6061Al alloy were solution-treated at 803 K for 2 h and quenched in a water bath quickly. The solution-treated materials were artificially aged at 448 K for different durations to study the effect of CNTs on the aging behavior.

2.3 Characterization of the CNT/6061Al Composites

Vickers hardnesses were measured on an automatic testing machine (LECO, LM-247AT) under a load of 100 g for 15 s. The hardness values at each condition were calculated by averaging ten test results. Dog-bone-shaped tensile specimens with a gauge length of 2.5 mm, a width of 1.5 mm and a thickness of 1 mm were machined from the FSP zones with the axis parallel to the FSP direction. Tensile tests were carried out at a strain rate of 1×10^{-3} s^{-1} at room temperature using an Instron 5848 tester. At least three specimens were tested for each material.

Scanning electron microscopy (SEM, Quanta 600) and field emission scanning electron microscopy (FESEM, Leo Supra 55) were used to observe the distribution of CNTs and the fracture surface of failed tensile specimens. Transmission electron microscopy (TEM, Tecnai G2 20) was used to observe the distribution of CNTs and the precipitate phases. CNT structure and CNT–Al interface were examined by high-resolution TEM (HRTEM). All TEM specimens were ion-milled with cooling device to avoid overheating during the ion-milling process.

3 Results and Discussion

3.1 Microstructure of the Composites

Figure 1a, b shows the distribution of CNTs in the forged CNT/6061Al composites with the CNT contents of 1.5 and 3 vol%. Clusters of CNTs with an average size of about 10 μm were observed, indicating that homogenous dispersion of CNTs cannot be achieved by simple mechanical mixing and hot forging. However, no clusters of CNTs could be found after FSP, at least under SEM, as shown in

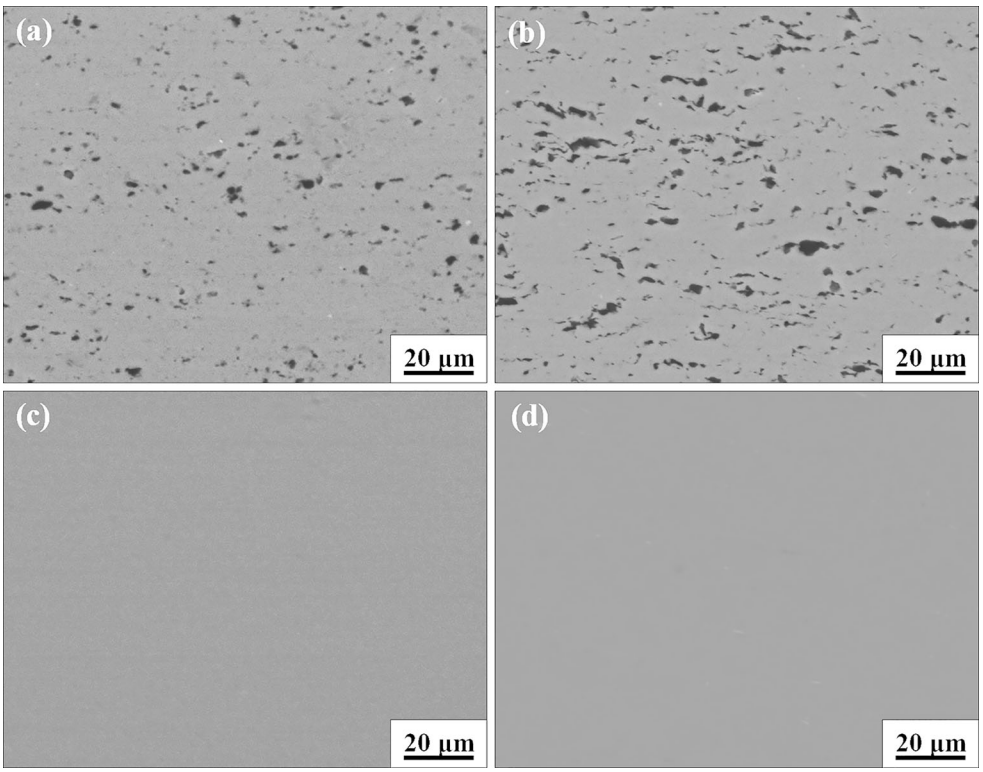

Fig. 1 CNT distribution in CNT/6061Al composites: **a**, **b** SEM images of forged 1.5, 3 vol% CNT/6061Al, **c**, **d** SEM images of FSP 1.5, 3 vol% CNT/6061Al

Fig. 1c, d, which indicated that the severe plastic deformation during FSP dispersed CNTs into the aluminum matrix.

Figure 2a shows the SEM image of the FSP 3 vol% CNT/6061Al composite. While some of the CNTs were singly dispersed, part of the CNTs was distributed in the matrix as fine CNT bundles consisting of several CNTs (about 2–4), which indicated that CNTs could be uniformly distributed into the aluminum matrix by FSP. Under TEM, the uniformly distributed CNTs in the aluminum matrix were obviously visible (Fig. 2b). It is noted that the lengths of CNTs in the composites were significantly shortened, which could be attributed to significant stirring and breakup effect during FSP. The entangled CNTs were firstly cut off by the shearing effect during FSP; then, the fragments were subsequently dispersed into the aluminum matrix due to the plastic flow of the aluminum matrix [8]. The diameters of CNTs in the FSP composite were estimated to be about 30 nm, similar to that of the as-received CNTs, indicating little damage of the tube wall structure of CNT.

Further observation under HRTEM indicated that CNTs still kept a tubular microstructure, as shown in Fig. 2c, d. The fracture of CNTs mainly occurred in the axis direction of CNTs; thus, the tube structure could still remain well after FSP. Furthermore, no pores were observed at the CNT–Al interfaces, as shown in Fig. 2d, which demonstrated the good interfacial bonding between CNTs and Al. The CNT structure integrity and good CNT–Al interfacial bonding play an important role in the load transferring, which is beneficial for the strengthening of CNT/Al composites.

3.2 Aging Behavior of the Composites

The FSP CNT/6061Al composites and FSP 6061Al were artificially aged for different durations after the solution treatment. The hardness values of the CNT/6061 composites and unreinforced 6061Al under different heat treatment conditions are shown in Fig. 3. After the solution treatment, the hardness of each material increased due to the solid solution of Mg and Si elements, compared to the FSP materials.

The hardness of 6061Al increased gradually with aging time and reached a maximum value after 10-h aging. As the aging duration further increased, the hardness of 6061Al exhibited a decreasing trend. The hardness of the CNT/6061Al composites exhibited a similar trend at the early stage of aging. However, the maximum hardness of 1.5 and 3 vol% CNT/6061Al composites were obtained after 8-h aging. It suggested that CNTs accelerated the precipitation process of the 6061Al matrix. Similar

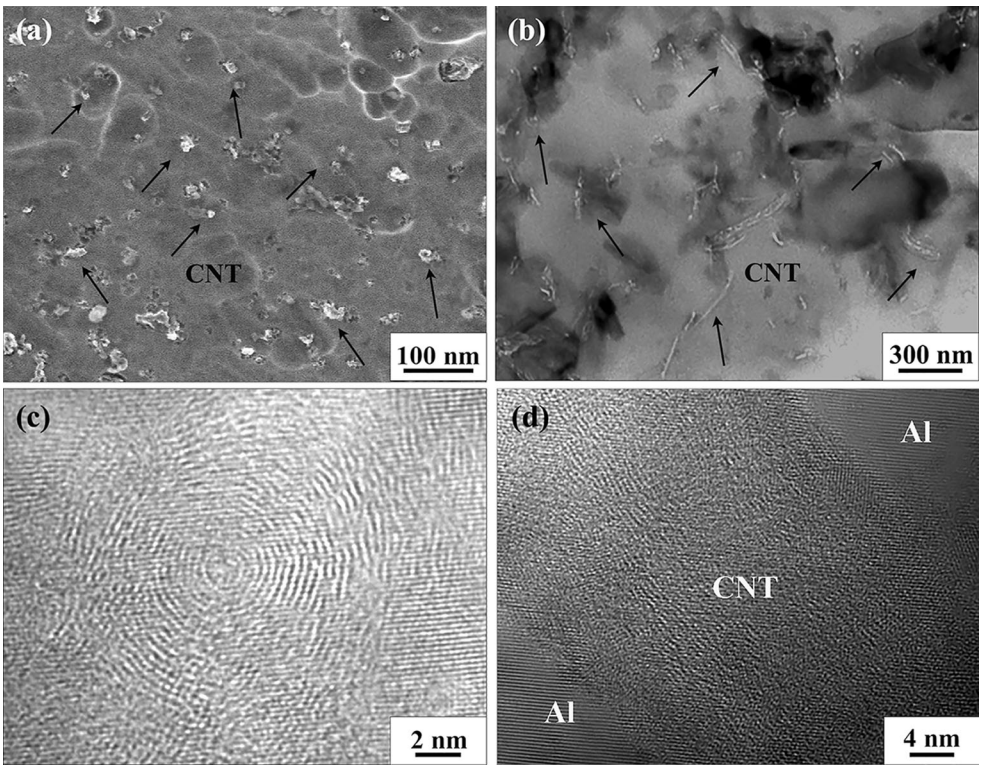

Fig. 2 **a** SEM and **b** TEM images showing CNT distribution in 3 vol% CNT/6061Al, **c**, **d** HRTEM images showing CNT structure and CNT–Al interface

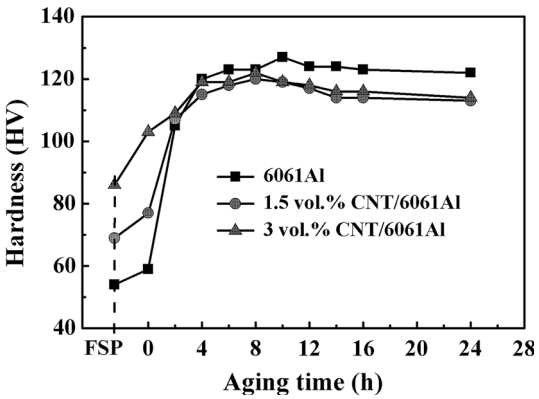

Fig. 3 Variation of hardness with aging time for 6061Al and CNT/6061Al composites

phenomenon has only been reported in the study of CNT/Al–4Cu composites fabricated by molecular-level mixing, and the generation of excess dislocations due to CNTs was thought to account for the accelerated precipitation process [21].

Under the FSP and solution treatment conditions, the hardness of CNT/6061Al composites increased with increasing the volume fraction of CNTs. However, under the T6 (peak aging) treatment condition, the CNT/6061Al composites had a slightly lower hardness compared to the 6061Al. It was deduced that the precipitation hardening in the aluminum alloy matrix has been negatively affected by the addition of CNTs.

XRD patterns of the 3 vol% CNT/6061Al composite under different heat treatment conditions are shown in Fig. 4. Peaks of Al_4C_3 were detected in all samples, indicating the damage of CNTs during the fabrication process. When the CNT clusters were mechanically broken down during FSP, many defects formed and the carbon atoms at the defect sites would react with the aluminum matrix to form Al_4C_3 phase. However, the low intensity of the peaks

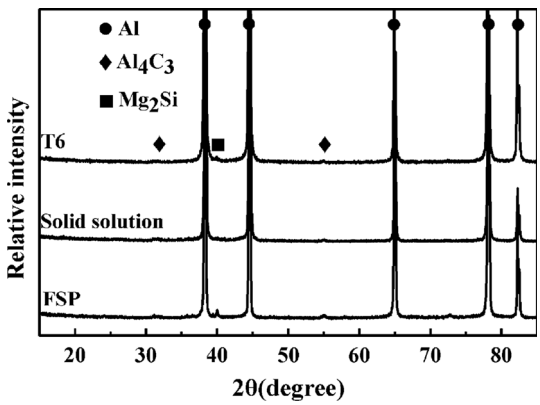

Fig. 4 XRD profiles of 3 vol% CNT/6061Al composites under different conditions

implied that the damage of CNTs introduced by FSP was very slight.

The precipitates in the T6-treated 3 vol% CNT/6061Al composite are shown in Fig. 5. In most of the matrix region, the precipitates with a needle shape were uniformly distributed. However, the precipitate-free zones (PFZs) were observed at the peripheral region of CNTs. The distance from PFZ boundaries to CNTs was about 45 nm. The strengthening effect of CNTs might be affected because the size of PFZs is far larger than the diameter of CNTs.

In previous studies [33–35], the PFZs around the grain boundaries of aged aluminum alloys, such as Al–Mg–Si and Al–Zn–Mg alloys, have been widely reported. This abnormal precipitation phenomenon has also been observed around reinforcements such as SiC, Al_2O_3 particles and whisker in MMCs [36–40]. However, this phenomenon has rarely been reported in the CNT/Al composites except our previous work [12].

The reason for the PFZ formation around CNTs has been analyzed in our previous study [12]. Due to the extremely large surface of CNTs, it is believed that the Mg and Si atoms were easy to segregate at the CNT boundaries and formed Mg_2Si particles because the CNT/Al interfaces had many dislocations and CNTs had some structure defects. This abnormal distribution of the precipitates was thought to account for the lower hardness of the T6-treated CNT/6061Al composites.

3.3 Mechanical Properties of the Composites Under Different Conditions

The yield strength (YS), ultimate tensile strength (UTS) and elongation (El) of the 6061Al and CNT/6061Al composites under different conditions are shown in Table 1.

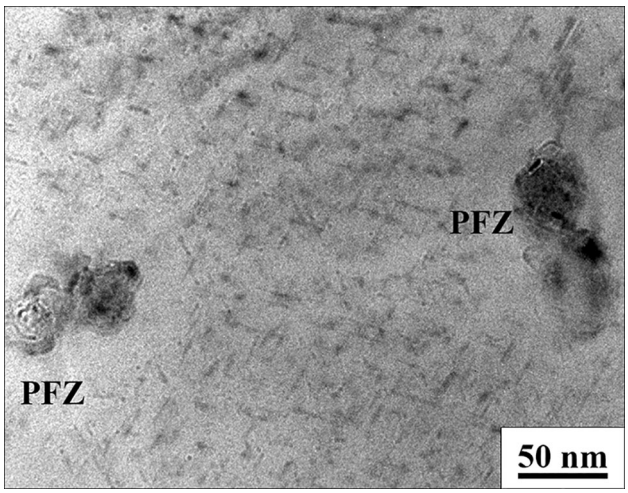

Fig. 5 TEM images showing precipitates in T6-treated CNT/6061Al composite

Table 1 Tensile properties of CNT/6061Al composites under different heat treatment conditions

CNT (vol%)	Condition	YS (MPa)	UTS (MPa)	El (%)
0	FSP	102 ± 3	190 ± 3	42 ± 1
1.5	FSP	130 ± 4	210 ± 5	31 ± 1
3	FSP	157 ± 5	253 ± 5	20 ± 2
0	Solution-treated	144 ± 3	250 ± 4	37 ± 2
1.5	Solution-treated	182 ± 3	287 ± 6	23 ± 1
3	Solution-treated	228 ± 5	317 ± 5	16 ± 1
0	T6-treated	300 ± 5	335 ± 3	28 ± 1
1.5	T6-treated	299 ± 6	353 ± 9	20 ± 2
3	T6-treated	291 ± 10	342 ± 11	14 ± 2

Under the FSP and solution treatment conditions, the strengthening effect of CNTs was significant. The YS of the FSP composites increased from 102 to 130 and 157 MPa as the CNT concentration increased from 0 to 1.5 and 3 vol%, respectively. For the solution-treated materials, the YS increased from 144 to 182 and 228 MPa as the CNT concentration increased from 0 to 1.5 and 3 vol%, respectively. This is thought to originate from the homogeneous dispersion of CNTs in the 6061Al matrix, as shown in Fig. 2.

However, under the T6 treatment condition, the strength of the composites showed insignificant or even no increment. This result was similar to the hardness trend of the T6-treated materials. In Nam's study [21], it was reported that CNTs could strengthen the Al–4Cu alloy matrix regardless of the heat treatment conditions, and no abnormal precipitate distribution was revealed. The insignificant strengthening effect of CNTs under the T6 treatment condition in our study might be attributed to the existence of the PFZs in the T6-treated CNT/6061Al composites (Fig. 5).

The YS of materials under the FSP and solution treatment conditions can be simply calculated by the generalized shear-lag model. After a mathematical transformation, the relationship between the YS and CNTs can be expressed as follows [21, 27]:

$$\sigma_C/\sigma_M - 1 = V_f S_{eff}. \quad (1)$$

where σ_M is the YS of the matrix, σ_C is the YS of the CNT/6061Al composites, V_f is the volume fraction of CNTs and S_{eff} is the effective aspect ratio of CNTs.

According to Eq. (1), the value of S_{eff} under the FSP and solution treatment conditions is 18.1 and 17.4, respectively. The closed S_{eff} values imply the similar strengthening efficiency under the FSP and solution treatment conditions. However, this calculation is unsuitable for the T6-treated CNT/6061Al composites due to the insignificant strengthening.

3.4 Modeling of the PFZ Effect on Composite Strength

A simple schematic, as shown in Fig. 6, can simply explain the strengthening effect of CNTs under different heat treatment conditions. Under the FSP and solution treatment conditions, the element distribution in the matrix was not affected by CNTs. Aluminum matrix was reinforced by the homogenously dispersed CNTs, thus enhancing mechanical properties. However, for the T6-treated composites the actual effective reinforcements changed, due to the existence of PFZs.

To analyze the effect of PFZs, a simple model is proposed for describing the effect of PFZs on the strength of the T6-treated CNT/6061Al composites. The T6-treated composites could be divided into two zones, as shown in Fig. 6b: (A) PFZs consisting of CNTs and (B) T6-treated 6061Al zones. PFZs could be considered as the actual effective reinforcements for the T6-treated CNT/6061Al composites.

Based on the TEM observation, the PFZs can be similarly considered as CNT/Al particles with a cylindrical shape and the distance from PFZ boundaries to CNTs (defined as W, as shown in Fig. 6b) was considered as a fixed value.

Strength of PFZs could be approximately estimated based on strength of the FSP CNT/Al composite (as shown in Table 2). For simplifying, the CNT/Al composites were also considered as PFZs-reinforced composites in order to access PFZs effect. Due to the same fabrication process, the distribution of CNTs and PFZs in the CNT/Al composite is seen to be same as those in the T6-treated CNT/6061Al composites.

Table 2 Tensile properties of FSP CNT/Al composites

CNT (vol%)	Condition	YS (MPa)	UTS (MPa)	El (%)
0	FSP	94	145	25 ± 1
1.5	FSP	133	181	20 ± 1

The volume fraction of the PFZs in the CNT/Al composites can be estimated by the volume ratio of the PFZs to CNTs. When CNTs are singly dispersed (that is, only single CNT existed in a PFZ), the volume fraction of the PFZs can be estimated by a simple geometric calculation, as follows:

$$\frac{V_{\mathrm{PFZ}}}{V_{\mathrm{CNT}}} = \frac{(2W + D)^2}{D^2} . \tag{2}$$

where V_{PFZ} is the volume fraction of PFZs, V_{CNT} is the volume fraction of CNTs, W is the distance from PFZ boundaries to CNTs and D is the diameter of CNTs.

However, some CNTs were formed fine bundles consisting of 2–4 CNTs, as shown in Fig. 2a. That is, part of the PFZs contained more than one CNT. Based on the observation of CNT distribution under SEM, the percentage of PFZs with different CNT numbers were counted, as shown in Table 3.

The calculation model of $V_{\mathrm{PFZ}}/V_{\mathrm{CNT}}$ for PFZs around variant CNT numbers is shown in Fig. 7. The distance from the PFZ boundaries to CNTs was still considered as a fixed value and was about 45 nm according to the TEM observation. For PFZs with different CNT numbers, the volume ratio of PFZ to CNT can also be calculated by geometric deduction.

To simplify the following descriptions, N is defined as the number of CNTs in a PFZ and the value is 1, 2, 3, 4 in

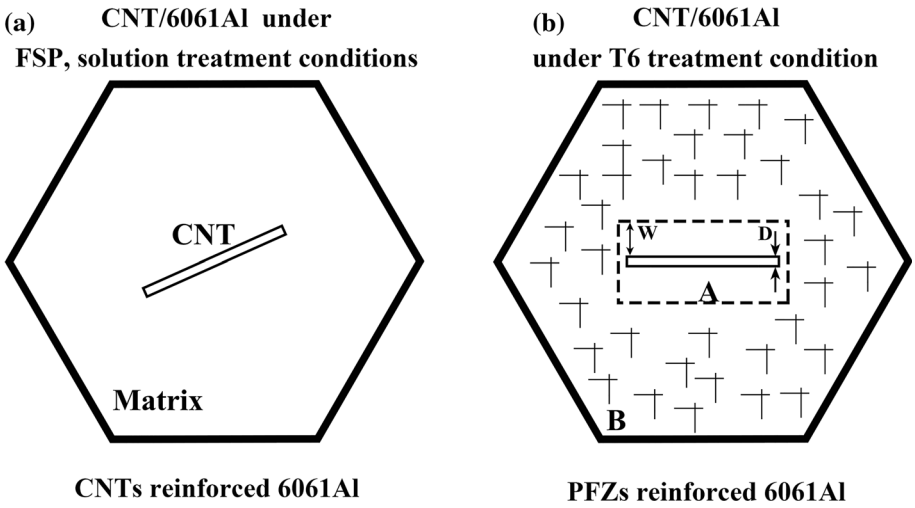

Fig. 6 Schematic showing the effective reinforcement changes under different conditions

Table 3 V_{PFZ}/V_{CNT} and the percentage of PFZs with different CNT numbers in PFZs

N (Number of CNTs in PFZs)	R_N (V_{PFZ}/V_{CNT})	P_N (Percentage)
1	16	0.37
2	12.5	0.33
3	8.7	0.19
4	7.3	0.11

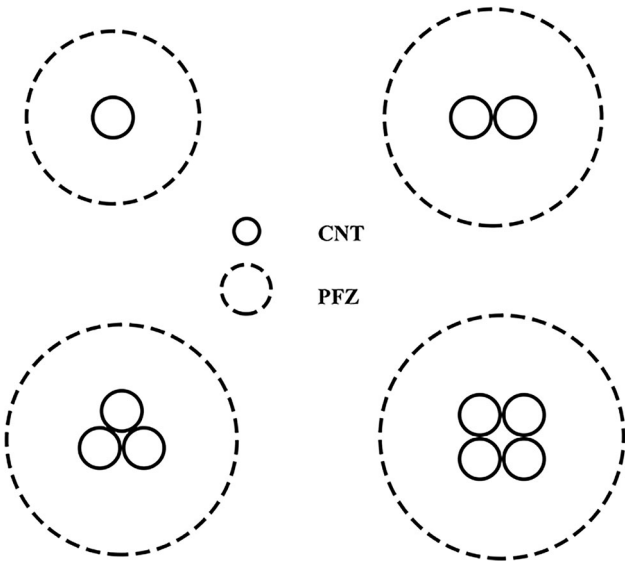

Fig. 7 Calculation schematic of V_{PFZ}/V_{CNT} for PFZs with different CNT numbers

this study. P_N is the percentage for PFZs with N CNTs. R_N represents the V_{PFZ}/V_{CNT} for PFZs with N CNTs. The values of N, P_N and R_N are summarized in Table 3 according to SEM observations.

Thus, the actual volume fraction of PFZs in the CNT/Al composite could be obtained as follows:

$$\frac{V_{PFZ}}{V_{CNT}} = P_1R_1 + P_2R_2 + P_3R_3 + P_4R_4. \quad (3)$$

From Eq. (3), the calculated V_{PFZ} is about 18.75% when V_{CNT} is 1.5%. That is, the 1.5 vol% CNT/Al composite could be regarded as 18.75 vol% PFZs/Al composite.

According to the rule of mixture, the average YS of PFZs (σ_{PFZ}) can be calculated from the following equation:

$$\sigma_c = \sigma_{PFZ}V_{PFZ} + \sigma_M(1 - V_{PFZ}). \quad (4)$$

For the 1.5 vol% CNT/Al composite, σ_c is 133 MPa, σ_M is 94 MPa, and V_{PFZ} is about 18.75%.

The calculated YS of PFZs was 282 MPa, slightly lower to the YS of the T6-treated 6061Al alloy. The UTS of PFZs could also be approximately calculated according to Eq. (4). The calculated UTS of PFZs was about 338 MPa, similar to the UTS of the T6-treated 6061Al alloy.

Although this calculation is simplified, the YS and UTS of PFZs were very similar to the T6-treated 6061Al matrix. As the T6-treated 6061Al was reinforced by PFZs which had similar strength, it was no doubt that the strengthening effect was insignificant.

The decreased ductility of T6-treated composites can also be explained by this model. According to the above calculation, the 1.5 vol% CNT/Al composite could be regarded as 18.75 vol% PFZs/Al composite, that is, the average content of CNT in PFZs was 8 vol%. In previous research [1, 41, 42], no plasticity could be observed when CNT/Al composites were reinforced by dispersed CNTs with CNT content above 6 vol%. The PFZs could be similarly considered as particles with very poor plasticity. As a result, the ductility of T6-treated composites decreased with the increasing content of PFZs.

Figure 8 shows the fractographs of the tensile specimens. Small dimples could be observed for the solution-treated and T6-treated composites. In bottom of the dimples, the solution-treated composite showed a flat morphology, with a few of pulled-out CNTs. By comparison, the T6-treated sample exhibited wrinkle morphology in bottom of the dimples. The results can also be explained by the local deformation of the PFZs.

The CNTs were pulled out during tension for the solution-treated composites, because the zones near the interface endured larger stress. However, for the T6-treated composites, PFZs around CNTs became other weak zones. Both the pulling out of CNTs and the fracture of PFZs occurred during tension. As a result, more complicated fracture morphology was produced. Similar phenomenon was reported in the aged SiC_p/7093Al composites [43–46]. Both particle fracture and near-interface deboning contributed to the failure of the aged composites due to the existence of PFZs around SiC_p. However, particle fracture was found to be dominant in the solution-treated composites.

In summary, PFZs had a negative effect on the mechanical properties of T6-treated CNT/6061Al composites. According to previous researches, the age-hardening ability of materials could be promoted by adding the concentration of alloy element [47, 48] and the morphology of PFZs was influenced by the heat treatment parameters, including aging temperature, aging time and solution treatment temperature [49, 50]. T6-treated CNT/6061Al composites with significant strengthening effect might be acquired by changing alloy element concentration and a series of complicated heat treatment.

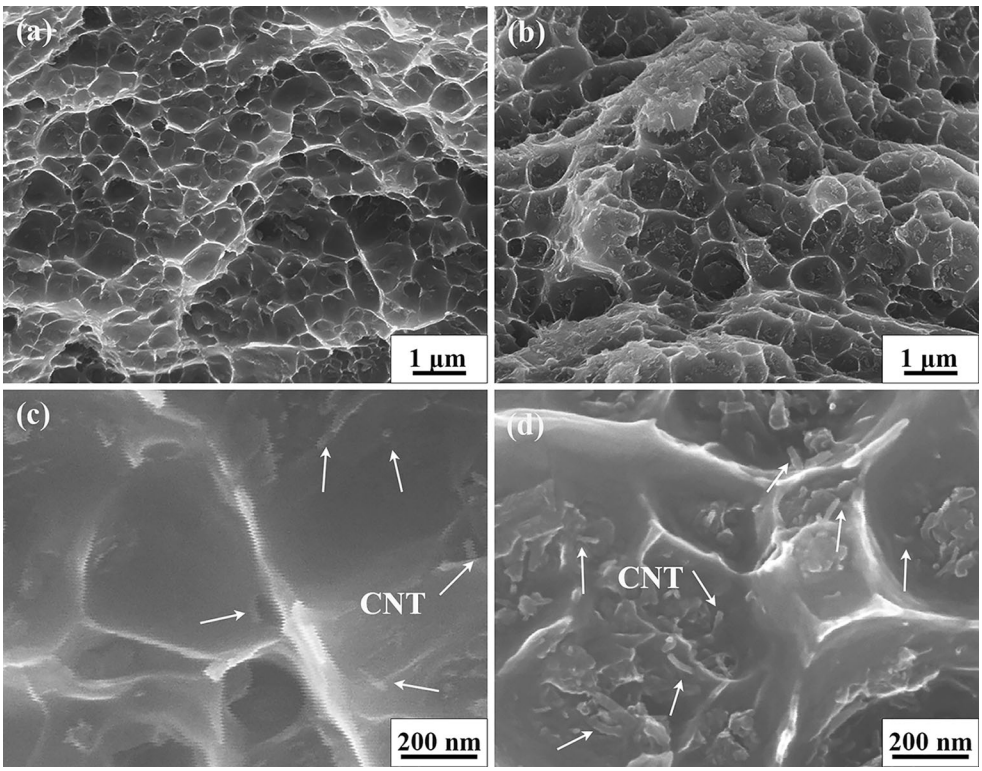

Fig. 8 Fracture morphology of 3 vol% CNT/6061Al composites: **a**, **c** solution-treated, **b**, **d** T6-treated

4 Conclusions

The CNT/6061Al composites with uniformly distributed CNTs were fabricated via PM combined with FSP. CNTs accelerated the precipitation process of CNT/6061Al composites, with the peak aging time being shortened from 10 to 8 h. Furthermore, PFZs with a distance of 45 nm from the PFZ boundaries to CNTs were detected around CNTs in the T6-treated CNT/6061Al composites.

The CNT/6061Al composites exhibited increased hardness and tensile strength compared to the 6061Al alloy under the FSP and solution treatment conditions. However, insignificant strengthening effect was observed for the T6-treated composites.

A model was proposed to describe the effect of PFZs on the strength of the T6-treated composites. The calculation indicated that the PFZs had similar strength to the T6-treated 6061Al, resulting in the insignificant strengthening effect.

Acknowledgements The authors gratefully acknowledge the support of National Key Research & Development Plan under Grant No.2017YFB0703100 and Key Research Program of Frontier Sciences, CAS, the CAS/SAFEA International Partnership Program for Creative Research Teams and the National Natural Science Foundation of China under Grant No. 51501189.

References

[1] S.R. Bakshi, D. Lahiri, A. Agarwal, Int. Mater. Rev. **55**, 41–64 (2010)
[2] A.M.K. Esawi, M.M. Farag, Mater. Des. **28**(9), 2394–2401 (2007)
[3] E.T. Thostenson, Z. Ren, T.-W. Chou, Compos. Sci. Technol. **61**(13), 1899–1912 (2001)
[4] P. Ajayan, O. Zhou, Appl. Carbon Nanotubes. **80**, 391–425 (2001)
[5] S.R. Bakshi, D. Lahiri, A. Agarwal, Int. Mater. Rev. **55**(1), 41–64 (2013)
[6] E. Neubauer, M. Kitzmantel, M. Hulman, P. Angerer, Compos. Sci. Technol. **70**(16), 2228–2236 (2010)
[7] W.A. Curtin, B.W. Sheldon, Mater. Today **7**(11), 44–49 (2004)
[8] Z.Y. Liu, B.L. Xiao, W.G. Wang, Z.Y. Ma, Carbon **50**(5), 1843–1852 (2012)
[9] R. Perez-Bustamante, F. Perez-Bustamante, I. Estrada-Guel, L. Licea-Jimenez, M. Miki-Yoshida, R. Martinez-Sanchez, Mater. Charact. **75**, 13–19 (2013)
[10] C. Biao, L. Shufeng, H. Imai, J. Lei, J. Umeda, M. Takahashi, K. Kondoh, Mater. Des. **72**, 1–8 (2015)
[11] L. Jiang, Z.Q. Li, G.L. Fan, L.L. Cao, D. Zhang, Carbon **50**(5), 1993–1998 (2012)
[12] Z.Y. Liu, B.L. Xiao, W.G. Wang, Z.Y. Ma, J. Mater. Sci. Technol. **30**(7), 649–655 (2014)
[13] D.H. Nam, S.I. Cha, B.K. Lim, H.M. Park, D.S. Han, S.H. Hong, Carbon **50**(7), 2417–2423 (2012)
[14] S. Simoes, F. Viana, M.A.L. Reis, M.F. Vieira, Compos. Struct. **108**, 992–1000 (2014)

[15] C.F. Deng, D.Z. Wang, X.X. Zhang, A.B. Li, Mater. Sci. Eng. A **444**(1–2), 138–145 (2007)
[16] J. Lipecka, M. Andrzejczuk, M. Lewandowska, J. Janczak-Rusch, K.J. Kurzydłowski, Compos. Sci. Technol. **71**(16), 1881–1885 (2011)
[17] A.M.K. Esawi, K. Morsi, A. Sayed, M. Taher, S. Lanka, Compos. A **42**(3), 234–243 (2011)
[18] H.J. Choi, J.H. Shin, D.H. Bae, Compos. Sci. Technol. **71**(15), 1699–1705 (2011)
[19] J. Lin, L. Zhiqiang, F. Genlian, C. Linlin, Z. Di, Scripta Mater. **66**(6), 331–334 (2012)
[20] L. Jiang, G. Fan, Z. Li, X. Kai, D. Zhang, Z. Chen, S. Humphries, G. Heness, W.Y. Yeung, Carbon **49**(6), 1965–1971 (2011)
[21] D.H. Nam, Y.K. Kim, S.I. Cha, S.H. Hong, Carbon **50**(13), 4809–4814 (2012)
[22] Z.Y. Liu, B.L. Xiao, W.G. Wang, Z.Y. Ma, Acta Metall. Sin. **27**(5), 901–908 (2014)
[23] D.K. Lim, T. Shibayanagi, A.P. Gerlich, Mater. Sci. Eng. A **507**(1–2), 194–199 (2009)
[24] Y. Morisada, H. Fujii, T. Nagaoka, M. Fukusumi, Mater. Sci. Eng. A **419**(1–2), 344–348 (2006)
[25] L.B. Johannes et al., Nanotechnology **17**(12), 3081 (2006)
[26] Z.Y. Liu, B.L. Xiao, W.G. Wang, Z.Y. Ma, Carbon **62**, 35–42 (2013)
[27] Z.Y. Liu, B.L. Xiao, W.G. Wang, Z.Y. Ma, Carbon **69**, 264–274 (2014)
[28] Z.Y. Liu, B.L. Xiao, W.G. Wang, Z.Y. Ma, Compos. Sci. Technol. **72**(15), 1826–1833 (2012)
[29] K. Kondoh, H. Fukuda, J. Umeda, H. Imai, B. Fugetsu, Carbon **72**, 15–21 (2014)
[30] C.H. Liu, X.L. Li, S.H. Wang, J.H. Chen, Q. Teng, J. Chen, Y. Gu, Mater. Des. **54**, 144–148 (2014)
[31] D. Maisonnette, M. Suery, D. Nelias, P. Chaudet, T. Epicier, Mater. Sci. Eng. A **528**(6), 2718–2724 (2011)
[32] H. Fukuda, K. Kondoh, J. Umeda, B. Fugetsu, Mater. Lett. **65**(11), 1723–1725 (2011)
[33] M. Raghavan, Metall. Trans. A **11**(6), 993–999 (1980)
[34] S.K. Hong, C.W. Won, D.H. Shin, K.K. Jee, S.I. Hong, Scripta Mater. **36**(8), 883–889 (1997)
[35] M.J. Starink, Mater. Sci. Eng. A **390**(1–2), 260–264 (2005)
[36] H. Toda, T. Kobayashi, M. Niinomi, J. Jpn. Inst. Met. **58**(4), 468–475 (1994)
[37] M.J. Starink, P.J. Gregson, Mater. Sci. Eng. A **211**(1–2), 54–65 (1996)
[38] G.E. Kiourtsidis, S.M. Skolianos, Corrosion **56**(6), 646–653 (2000)
[39] R. Nagarajan, I. Dutta, Metall. Mater. Trans. A **32**(2), 433–436 (2001)
[40] T. Kobayashi, H. Toda, Mater. Sci. Forum **217–222**, 1127–1132 (1996)
[41] T. Sie Chin, Mater. Sci. Eng. R **74**(10), 281–350 (2013)
[42] R. Casati, M. Vedani, Metals **4**(1), 65–83 (2014)
[43] M.J. Starink, S. Syngellakis, Mater. Sci. Eng. A **270**(2), 270–277 (1999)
[44] M.J. Starink, P. Wang, I. Sinclair, P.J. Gregson, Acta Mater. **47**(14), 3855–3868 (1999)
[45] M.J. Starink, P. Wang, I. Sinclair, P.J. Gregson, Acta Mater. **47**(14), 3841–3853 (1999)
[46] A.B. Pandey, B.S. Majumdar, D.B. Miracle, Metall. Mater. Trans. A **31**(3A), 921–936 (2000)
[47] Y.Z. Li, Q.Z. Wang, W.G. Wang, B.L. Xiao, Z.Y. Ma, Mater. Chem. Phys. **154**, 107–117 (2015)
[48] Y.Z. Li, Q.Z. Wang, W.G. Wang, B.L. Xiao, Z.Y. Ma, Mater. Sci. Eng. A **620**, 445–453 (2015)
[49] Y.Q. Xu, L.H. Zhan, S.J. Li, X.T. Wu, Rare Met. Mater. Eng. **46**(2), 355–362 (2017)
[50] J. Song, R. Field, D. Konitzer, M. Kaufman, Metall. Mater. Trans. A **48A**(5), 2425–2434 (2017)